Journal of The Electrochemical Society

The Electrochemical Society
Advancing solid state & electrochemical science & technology

OPEN ACCESS

Proton and Electron Transport Impedance of Inactive Catalyst Layer Embedded in PEM Fuel Cell

To cite this article: Andrei Kulikovsky 2021 *J. Electrochem. Soc.* **168** 034501

Journal of The Electrochemical Society, 2021 **168** 034501

Proton and Electron Transport Impedance of Inactive Catalyst Layer Embedded in PEM Fuel Cell

Andrei Kulikovsky[1,2,*,z]

[1]*Theory and Computation of Energy Materials (IEK-13), Institute of Energy and Climate Research, Forschungszentrum Jülich GmbH,D–52425 Jülich, Germany*
[2]*Lomonosov Moscow State University, Research Computing Center, 119991 Moscow, Russia*

Placing a catalyst layer between two membranes in a PEM fuel cell one gets a membrane–electrode assembly with inactive catalyst layer (ICL). A model for ICL impedance is developed taking into account finite electron conductivity of the layer. Analytical expression for the ICL impedance is derived. Analysis of characteristic features of the ICL Nyquist spectrum leads to simple analytical expressions for the high–frequency and polarization resistivity, for the summit frequency and for the straight high–frequency part of the spectrum. The results allow to estimate the ICL proton and electron conductivities and double layer capacitance without complicated curve fitting.

 [DOI: 10.1149/1945-7111/abe7a4]

Manuscript submitted November 11, 2020; revised manuscript received January 26, 2021. Published March 1, 2021.

List of symbols

~	Marks dimensionless variables
b_*	Thermal potential, RT/F, V
C_{dl}	Double layer volumetric capacitance, F cm^{-3}
f	Regular frequency, Hz
j_0	Cell current density, A cm^{-2}
j_e	Electron current density, A cm^{-2}
j_e^*	Characteristic current density of electron transport, A cm^{-2}, Eq. 1
j_p	Proton current density, A cm^{-2}
j_p^*	Characteristic current density of proton transport, A cm^{-2}, Eq. 1
i	Imaginary unit
k_σ	Ratio of electron and proton conductivities, Eq. 15
l_t	Catalyst layer thickness, cm
R_{icl}	ICL total resistivity, Ω cm^2
R_{icl}^{hfr}	ICL high–frequency resistivity, Ω cm^2
R_{icl}^{pol}	ICL polarization resistivity, Ω cm^2
t	Time, s
x	Coordinate through the CL, cm
Z_{acl}	Impedance of active CL, Ω cm^2
Z_{icl}	Impedance of inactive CL, Ω cm^2

Subscripts

a	Active material
acl	Active catalyst layer
e	Electron
dl	Double layer
icl	Inactive catalyst layer
im	Imaginary part
p	Proton
re	Real part
t	Catalyst layer

Superscripts

hfr	High frequency resistivity
pol	Polarization (resistivity)
*	Characteristic value; ACL parameters in Section III E

Greek

η	Overpotential, $\eta = \Phi - \phi$, V
σ_e	CCL electronic conductivity, Ω^{-1} cm^{-1}
σ_p	CCL ionic conductivity, Ω^{-1} cm^{-1}
ξ	Dimensionless parameter, Eq. 22
Φ	Membrane phase potential, V
ϕ	Carbon phase potential, V
ω	Angular frequency ($\omega = 2\pi f$), s^{-1}
$\omega_{\max}$	Summit frequency of Nyquist spectrum, s^{-1}

Transport of charged species to oxygen reduction reaction sites is important function of the cathode catalyst layer (CCL) in a PEM fuel cell. Ideally, this transport should be fast, meaning that the respective potential loss is negligible. This condition holds if the characteristic current densities for proton j_p^* and electron j_e^* transport are much larger, than the working current density j_0 of the cell:

$$j_0 \ll \min\left\{j_p^* = \frac{\sigma_p b}{l_t},\quad j_e^* = \frac{\sigma_e b}{l_t}\right\} \qquad [1]$$

Here, σ_p, σ_e are the CCL proton and electron conductivities, b is the ORR Tafel slope, and l_t is the CCL thickness. In addition to direct ohmic loss, poor proton transport causes formation of the ORR rate peak at the membrane surface leaving the rest part of the CCL inactive. Such a strongly non–uniform shape of the ORR rate dramatically lowers the cell potential.[1,2] This effect explains large interest in measuring σ_p in CCLs (see a recent review[3]).

In PEMFC studies, CCL electron conductivity took much less attention; mostly due to common belief that σ_e is much higher than σ_p and hence the potential loss due to σ_e can be ignored. This, however, is not necessarily the case: CCL electron transport properties strongly depend on ionomer/carbon ratio and for some compositions, σ_e as low as 1 mS cm^{-1} has been reported.[4] More references on measuring σ_e in PEMFC CCLs can be found in Refs. 4, 5. The problem of catalyst layer electron conductivity is particularly severe in water electrolysis cells. Due to high rate of carbon corrosion, these cells employ Ir–or Ti–based catalyst supports, which typically have lower σ_e, than carbon–based support.[6–8] Detailed analysis of relevant numerical and analytical impedance models has been given in Ref. 9.

Measuring of σ_p in the CCL is usually performed by means of electrochemical impedance spectroscopy (EIS) of the cell running in H_2/N_2 regime.[10–15] External voltage is applied to generate protons

*Electrochemical Society Member.
[z]E-mail: A.Kulikovsky@fz-juelich.de

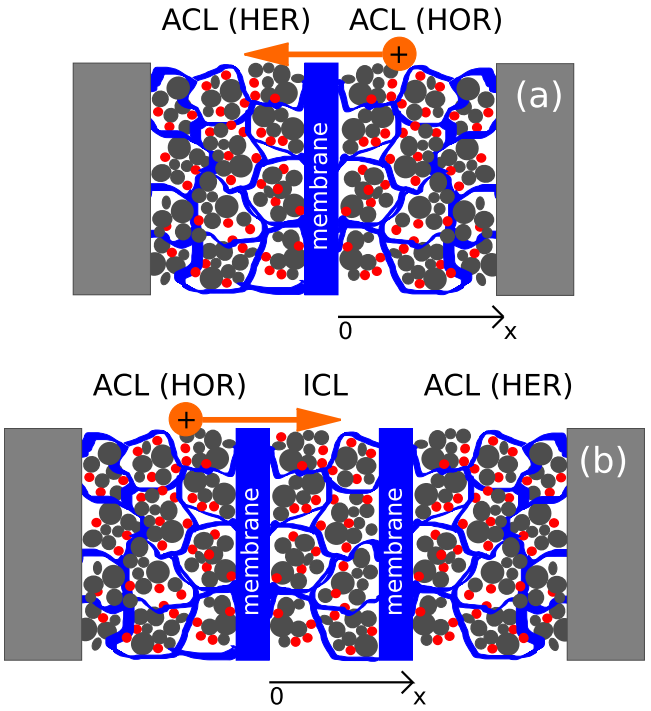

Figure 1. Schematic for measuring impedance of the cell in (a) H_2/N_2regime and (b) proton pumping regime. ACL stands for active catalyst layer, and ICL denotes inactive catalyst layer (ICL).

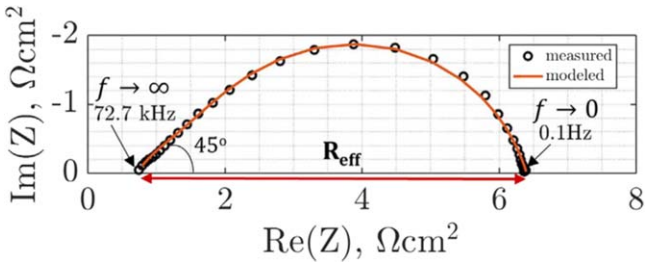

Figure 2. Nyquist spectrum of inactive CL. Reprinted from Ref. 16.

on the cell cathode by oxidation of hydrogen permeated through the membrane. Under the applied electric field, protons move to the cell anode, where they recombine with electrons in the hydrogen evolution reaction (HER) (Fig. 1a). While the contribution of HOR and HER is typically negligible, the reactions generate proton current in the membrane, which shifts the H_2/N_2 Nyquist spectrum due to the so–called membrane high–frequency resistance (HFR). Below, we will show that the membrane HFR masks the electrode contribution to the HFR.

Proton conductivity is extracted from the measured spectra either by fitting a classic de Levie equation for impedance of the single pore to the measured spectra,[13,14] or simply by using relations between the layer ionic resistivity and capacitance, which follow from de Levie formula.[10–12] A comprehensive review of impedance models for the porous electrode, including discussion of applicability of de Levie equation has recently been published by Huang et al.[17]

Following ideas of Boyer et al.,[18] Iden et al.[19,20] and Kramer et al.,[21] Sabarirajan et al.[16] used another approach for measuring catalyst layer impedance. A standard CCL is placed between two membranes and embedded into the fuel cell environment (Fig. 1b). The cell is operated in hydrogen pumping regime with the hydrogen oxidation reaction (HOR) on the left electrode and HER on the right electrode. Due to separating membranes, the layer in between is disconnected from electron transport and hence no electrochemistry runs in the layer. Following terminology of Boyer et al., below this layer will be referred to as inactive catalyst layer (ICL). Sabarirajan et al.[16] measured impedance of the cell in Fig. 1b; the typical spectrum is shown in Figure 2. Assuming infinite electron conductivity of the ICL, they fitted equivalent circuit impedance to experimental spectra and reported proton conductivity of the ICL. Not questioning the results of Sabarirajan et al.,[16] it is worth mentioning that the equivalent circuit approach may lead to irrelevant results, as discussed by Macdonald in his seminal paper.[22]

In this work, we derive and analyze analytical expression for ICL impedance resulting from a physics–based model, which takes into account finite ICL electron conductivity. In the limit of large ratio of electron to proton conductivity, explicit relations for the proton and electron transport impedance of the ICL are obtained. The ICL impedance is compared to the active catalyst layer impedance in the standard H_2/N_2 setup in Fig. 1a. Analytical relation for the ICL impedance can be used for fitting experimental spectra. Furthermore, obtained relations between the characteristic points of the Nyquist spectrum and the ICL parameters allow one to estimate the conductivities of charged species and double layer capacitance without curve fitting.

Model

Basic equations.—Below, ACL denotes active catalyst layer, no matter what reaction runs in this layer. In the H_2/N_2 regime, the cell cathode performs HOR, while the cell anode runs HER. In the hydrogen pumping regime, the cell anode runs HOR and the cathode HER. However, the impedance of HOR and HER electrodes is described by the same equation, while the ICL impedance is quite different due to different set of boundary conditions for the problem (see below).

Regardless of the boundary conditions, the transient conservation equations for the proton and electron charge in the ACL and ICL are

$$C_{dl}\frac{\partial \eta}{\partial t} + \frac{\partial j_p}{\partial x} = 0 \qquad [2]$$

$$C_{dl}\frac{\partial \eta}{\partial t} + \frac{\partial j_e}{\partial x} = 0 \qquad [3]$$

where t is time, x is the distance through the layer counted from the membrane (Fig. 1), C_{dl} is the double layer volumetric capacitance, η is the overpotential

$$\eta = \Phi - \phi \qquad [4]$$

and j_p and j_e are the local proton and electron current densities subject to the Ohm's law

$$j_p = -\sigma_p \frac{\partial \Phi}{\partial x} \qquad [5]$$

$$j_e = \sigma_e \frac{\partial \phi}{\partial x}. \qquad [6]$$

Here, Φ is the membrane phase potential, ϕ is the carbon phase (electronic) potential. j_p and j_e are related by

$$j_p(x) - j_e(x) = j_0 \qquad [7]$$

where j_0 is the cell current density. Note that here, j_p and j_e are the fluxes of protons and electrons, respectively, multiplied by the unsigned electron charge.

Ohm's law allows us to eliminate current densities from Eqs. 2, 3, and these equations transform to

$$C_{dl}\frac{\partial\eta}{\partial t} - \sigma_p\frac{\partial^2\Phi}{\partial x^2} = 0, \quad [8]$$

$$C_{dl}\frac{\partial\eta}{\partial t} + \sigma_e\frac{\partial^2\phi}{\partial x^2} = 0, \quad [9]$$

Strictly speaking, in the cell operating under H_2/N_2 feed, Eqs. 8 and 9, describe the open–circuit regime of the ACL function. Usually, however, hydrogen crossover takes place through the membrane and to oxidize the hydrogen flux, an external potential on the order of hundred millivolts or more is applied to the cell. This potential produces huge HOR overpotential on the cell cathode, forcing HOR to run in a very thin sub–layer close to the membrane interface. The proton current due to crossover is small (typically, below 3 mA cm^{-2}) and hence the faradaic HOR impedance in the ACL can be safely ignored. In the ICL, no electrochemistry runs at all. Therefore, in the bulk of the ACL and in the ICL, Eqs. 8 and 9 describe AC signal–induced periodic oscillations of protons and electrons around their equilibrium positions at the Pt-C/electrolyte interface. From the EIS standpoint, running constant proton current through the ICL is not necessary, as the system impedance can be measured at zero DC current.

It is convenient to introduce dimensionless variables

$$\tilde{x} = \frac{x}{l_t}, \quad \tilde{t} = \frac{t}{t_*}, \quad \tilde{\Phi} = \frac{\Phi}{b_*}, \quad \tilde{\phi} = \frac{\phi}{b_*}, \quad \tilde{\eta} = \frac{\eta}{b},$$
$$\tilde{j} = \frac{j}{j_p^*}, \quad \tilde{Z} = \frac{Z\sigma_p}{l_t}, \quad \tilde{\omega} = \omega t_* \quad [10]$$

where $b_* = RT/F$, $\omega = 2\pi f$ is the angular frequency of the applied signal and

$$t_* = \frac{C_{dl}l_t^2}{\sigma_p} \quad [11]$$

is the scaling parameter for time. With the parameters 10, Eqs. 8, 9 transform to

$$\frac{\partial\tilde{\eta}}{\partial\tilde{t}} - \frac{\partial^2\tilde{\Phi}}{\partial\tilde{x}^2} = 0 \quad [12]$$

$$\frac{\partial\tilde{\eta}}{\partial\tilde{t}} + k_\sigma\frac{\partial^2\tilde{\phi}}{\partial\tilde{x}^2} = 0 \quad [13]$$

where

$$\tilde{\eta} = \tilde{\Phi} - \tilde{\phi} \quad [14]$$

and

$$k_\sigma = \frac{\sigma_e}{\sigma_p}. \quad [15]$$

Equations 12, 13 are linear and since Fourier transform converts time derivatives $\partial\tilde{\eta}^1/\partial\tilde{t}$ into products $i\tilde{\omega}\tilde{\eta}^1$, we can immediately write down equations for the small perturbation amplitudes in the omega–space $\tilde{\Phi}^1$ and $\tilde{\phi}^1$ marked by the superscript 1:

$$\frac{\partial^2\tilde{\Phi}^1}{\partial\tilde{x}^2} = i\tilde{\omega}(\tilde{\Phi}^1 - \tilde{\phi}^1) \quad [16]$$

$$k_\sigma\frac{\partial^2\tilde{\phi}^1}{\partial\tilde{x}^2} = -i\tilde{\omega}(\tilde{\Phi}^1 - \tilde{\phi}^1) \quad [17]$$

This pair of equations determines evolution of small–amplitude AC perturbations in the system. Specific features of the system environment (ACL or ICL) are described by the boundary conditions.

Active catalyst layer impedance.—For further references, in this subsection we re–derive the expression for impedance of the active (cathode) catalyst layer in a cell operated in H_2/N_2 regime. In the ACL running HOR, the proton current is zero at the ACL/GDL interface, while electron current is zero at the membrane/ACL interface. The system 16, 17 thus obeys to the boundary conditions

$$\tilde{\Phi}^1(0) = 0, \quad \left.\frac{\partial\tilde{\Phi}^1}{\partial\tilde{x}}\right|_{\tilde{x}=1} = 0 \quad [18]$$

$$\left.\frac{\partial\tilde{\phi}^1}{\partial\tilde{x}}\right|_{\tilde{x}=0} = 0, \quad \tilde{\phi}(1) = \tilde{\phi}_1^1 \quad [19]$$

where $\tilde{\phi}_1^1$ is the amplitude of applied AC perturbation of potential. The ACL impedance is given by

$$\tilde{Z}_{acl} = \left.\frac{\tilde{\phi}^1}{k_\sigma\partial\tilde{\phi}^1/\partial\tilde{x}}\right|_{\tilde{x}=1} \quad [20]$$

Solution of the linear system 16— 19 with constant coefficients can be obtained using any math software, e.g. Maple®. Calculating impedance with Eq. 20, we get

$$\tilde{Z}_{acl} = \frac{1}{1+k_\sigma} + \frac{2 + (k_\sigma + 1/k_\sigma)\cosh\xi}{(1+k_\sigma)\xi\sinh\xi} \quad [21]$$

where

$$\xi = \sqrt{i\tilde{\omega}\left(1 + \frac{1}{k_\sigma}\right)}. \quad [22]$$

The impedance 21 is equivalent to Eq. (13) in Ref. 23, where it has been analyzed in detail.

Results and Discussion

Inactive catalyst layer impedance.—In the case of ICL, solution of the system 16, 17 obeys to the following boundary conditions:

$$\left.\frac{\partial\tilde{\Phi}^1}{\partial\tilde{x}}\right|_{\tilde{x}=0} = -\tilde{j}_1^1, \quad \tilde{\Phi}^1(1) = 0 \quad [23]$$

$$\left.\frac{\partial\tilde{\phi}^1}{\partial\tilde{x}}\right|_{\tilde{x}=0} = 0, \quad \left.\frac{\partial\tilde{\phi}^1}{\partial\tilde{x}}\right|_{\tilde{x}=1} = 0 \quad [24]$$

where $\tilde{j}_1^1$ is the amplitude of applied perturbation of proton current density entering the ICL. Equations 23 mean that the perturbation of proton current comes from the left (HOR) side of the cell (Fig. 1b), while zero reference point for potentials is fixed at the right membrane interface ($\tilde{x} = 1$). Equations 24 express zero electron current at the ICL/membrane interface, on either side of the ICL.

The ICL impedance is determined by

$$\tilde{Z}_{icl} = \left.\frac{\tilde{\Phi}^1}{\tilde{j}_1^1}\right|_{\tilde{x}=0}. \quad [25]$$

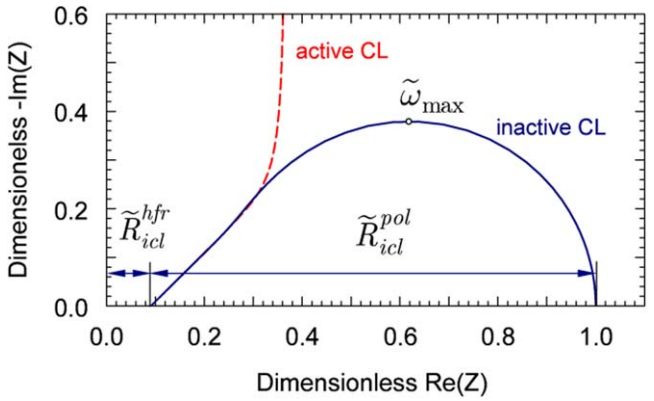

Figure 3. Nyquist spectra of the inactive catalyst layer (solid curve), and of the active catalyst layer of the cell operated in H_2/N_2 regime (dashed curve).

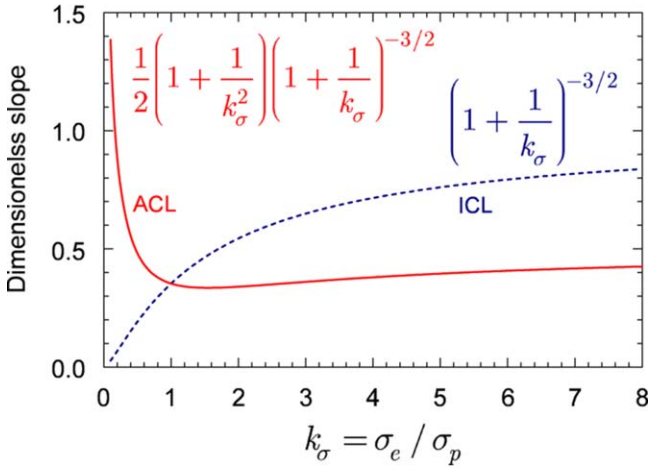

Figure 4. The slope of the straight line $\tilde{Z}_{im}$ vs $\sqrt{2/\tilde{\omega}}$ in the high–frequency domain (the factors at $\sqrt{2/\tilde{\omega}}$ in Eqs. 35, 36, 37, 38). Solid curve: ACL, dashed curve: ICL.

Solution of the system 16, 17, 23, 24 gives

$$\tilde{Z}_{icl} = \frac{1}{1+k_\sigma} + \frac{2(\cosh(\xi)-1)}{(1+1/k_\sigma)\xi\sinh\xi} \qquad [26]$$

where ξ is given by Eq. 22. In the limit of large σ_e, $k_\sigma \to \infty$ and the ICL impedance 26 simplifies to

$$\tilde{Z}_{icl}^{k_\sigma=\infty} = \frac{2(\cosh(\sqrt{i\tilde{\omega}})-1)}{\sqrt{i\tilde{\omega}}\sinh\sqrt{i\tilde{\omega}}} \qquad [27]$$

which is a pure proton transport impedance. Note that the ICL high–frequency resistivity (the first term in Eq. 26) vanishes in this limit.

The spectra of $\tilde{Z}_{acl}$, Eq. 21, and $\tilde{Z}_{icl}$, Eq. 26, are compared in Fig. 3. The ACL spectrum exhibits capacitive behavior as $\tilde{\omega}$ decreases. On the contrary, the ICL spectrum at lower frequencies is similar in shape, but not equal to the finite–length Warburg transport arc. Of particular interest are the characteristic points of the ICL spectrum. At large frequency, $\xi \to \infty$, the second term in Eq. 26 tends to zero and the leftmost point of the ICL Nyquist spectrum (the ICL high–frequency resistivity) is given by

$$\tilde{R}_{icl}^{hfr} = \frac{1}{1+k_\sigma}, \quad R_{icl}^{hfr} = \frac{l_t}{\sigma_p+\sigma_e} \qquad [28]$$

(Fig. 3). Rewriting the latter expression as

$$\frac{1}{R_{icl}^{hfr}} = \frac{1}{l_t/\sigma_p} + \frac{1}{l_t/\sigma_e} \qquad [29]$$

we see that Eq. 28 is equivalent to the proton and electron ICL resistivities connected in parallel. The same HFR has the active layer spectrum, Eq. 21.

It is important to note that the measured high–frequency resistance R_{cell}^{hfr} of a cell with the ICL would contain the contribution from membrane/contact resistances R_m, and the contributions from active layers:

$$R_{cell}^{hfr} = R_{icl}^{hfr} + R_m + 2R_{acl}^{hfr} \qquad [30]$$

This makes it difficult, if not impossible separation of the ICL contribution R_{icl}^{hfr} from the measured HFR.

In the opposite limit of zero frequency, the impedance $\tilde{Z}_{icl}$ reduces to the total system resistivity

$$\tilde{R}_{icl} = \frac{1}{1+k_\sigma} + \frac{1}{1+1/k_\sigma} \qquad [31]$$

which in the dimension form reads

$$R_{icl} = \frac{l_t}{\sigma_p+\sigma_e} + \frac{l_t}{\sigma_p(1+\sigma_p/\sigma_e)} \qquad [32]$$

The second term in Eq. 32 is the ICL polarization resistivity

$$R_{icl}^{pol} = \frac{l_t}{\sigma_p(1+\sigma_p/\sigma_e)} \qquad [33]$$

The value of R_{icl}^{pol} is easy to obtain from experiment simply by measuring the arc diameter (Fig. 3). The ICL thickness l_t is usually known, hence R_{icl}^{pol} relates two unknown parameters, σ_p and σ_e. In the limit of large σ_e ($\sigma_e/\sigma_p \gtrsim 10$), the second term in denominator of Eq. 33 is small, and σ_p can be estimated simply as

$$\sigma_p \simeq \frac{l_t}{R_{icl}^{pol}} \qquad [34]$$

Note that finite k_σ lowers the ICL polarization resistivity and it increases the HFR resistivity, as Eq. 31 shows. This effect is due to negative differential resistivity of electronic component, which is discussed in detail in Section III D.

High–frequency inactive CL impedance.—To obtain high–-frequency asymptotic for ICL impedance we first calculate $\mathrm{Re}\,(\tilde{Z}_{icl})$; the resulting expression contains trigonometric and hyperbolic functions of ξ. In the limit of large $\tilde{\omega}$, $\xi \to \infty$ and for the hyperbolic functions we may retain leading exponent only, $\cosh(\xi) \simeq \sinh(\xi) \simeq \exp(\xi)/2$. Making this substitutions and neglecting the terms with $\exp(-\xi)$, we come to

$$\tilde{Z}_{icl,re}^{\tilde{\omega}\to\infty} \simeq \frac{1}{1+k_\sigma} + \left(1+\frac{1}{k_\sigma}\right)^{-3/2}\sqrt{\frac{2}{\tilde{\omega}}} \qquad [35]$$

Quite analogous manipulations with imaginary part of $\tilde{Z}_{icl}$ lead to

$$\tilde{Z}_{icl,im}^{\tilde{\omega}\to\infty} \simeq \left(1+\frac{1}{k_\sigma}\right)^{-3/2}\sqrt{\frac{2}{\tilde{\omega}}} \qquad [36]$$

In Nyquist coordinates, Eqs. 35, 36 describe the straight line with the 45° slope; the line is shifted from the origin of coordinates by the resistivity $\tilde{R}_{icl}^{hfr}$ (Fig. 3).

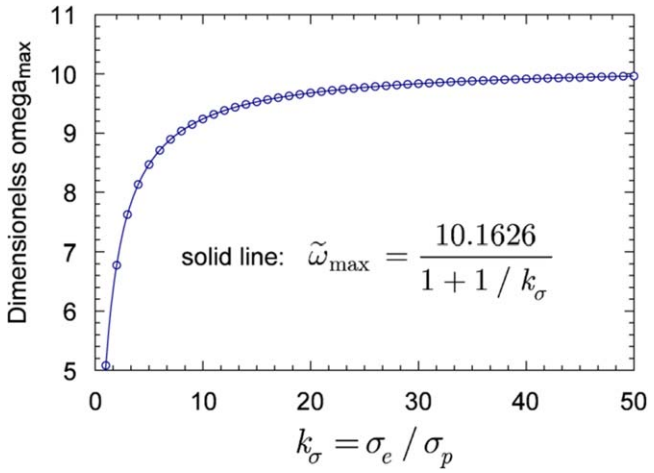

Figure 5. Open circles—exact numerical dimensionless angular frequency $\tilde{\omega}_{max}$ corresponding to the peak value of imaginary part of impedance $\max\{-\tilde{Z}_{im}\}$. Solid line shows the best–fit equation, Eq. 39.

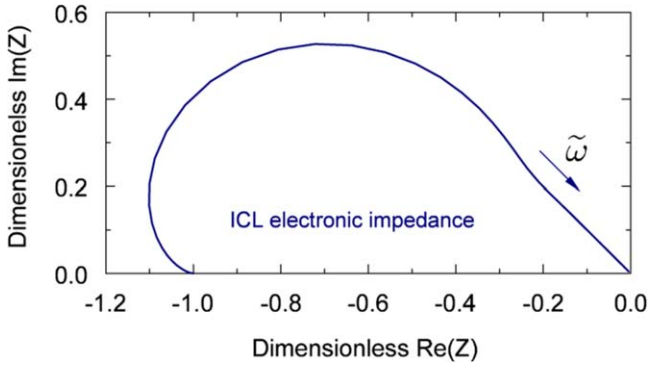

Figure 6. Nyquist spectrum of ICL electronic impedance, Eq. 42, multiplied by k_σ.

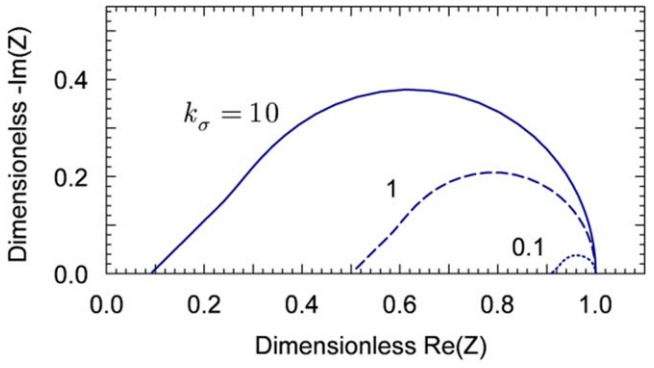

Figure 7. ICL Nyquist spectra for the indicated values of parameter $k_\sigma = \sigma_e/\sigma_p$.

It is interesting to compare Eqs. 35, 36 with the high–frequency equations for the real and imaginary part of the active catalyst layer impedance which can be derived from asymptotic expansion of Eq. 21 for $k_\sigma \to \infty$

$$\tilde{Z}_{acl,re}^{\tilde{\omega}\to\infty} \simeq \frac{1}{1+k_\sigma} + \frac{1}{2}\left(1+\frac{1}{k_\sigma^2}\right)\left(1+\frac{1}{k_\sigma}\right)^{-3/2}\sqrt{\frac{2}{\tilde{\omega}}} \qquad [37]$$

$$\tilde{Z}_{acl,im}^{\tilde{\omega}\to\infty} \simeq \frac{1}{2}\left(1+\frac{1}{k_\sigma^2}\right)\left(1+\frac{1}{k_\sigma}\right)^{-3/2}\sqrt{\frac{2}{\tilde{\omega}}} \qquad [38]$$

Comparing Eqs. 35, 36 with Eqs. 37, 38, we see that in Nyquist coordinates, both pairs of equations describe the straight 45°–line. Suppose now that we plot the imaginary component of ACL and ICL impedance vs $\sqrt{2/\tilde{\omega}}$. At high frequencies, we would get the straight line with the *slope* depending on k_σ (Fig. 4). The slopes for the ACL and ICL differ by the factor $\frac{1}{2}\left(1+\frac{1}{k_\sigma^2}\right)$, which rapidly tends to 1/2 as k_σ increases. Note that as $k_\sigma \to 0$, the ACL slope increases to infinity, while the ICL slope decreases to zero (Fig. 4). Note also that the ACL curve has minimum at $k_\sigma = (2+\sqrt{7})/3 \simeq 1.549$ (Fig. 4). Substitutions $\tilde{Z} = Zl_t/\sigma_p$, and $\tilde{\omega} = \omega C_{dl} l_t^2/\sigma_p$ transform Eqs. 35, 36 into their dimension form (Appendix), which can be used for practical calculations of σ_p, σ_e and C_{dl}.

Summit frequency of the Nyquist spectrum.—A useful relation between the ICL parameters gives the summit frequency $\tilde{\omega}_{max}$ corresponding to the top point of the Nyquist spectrum (Fig. 3). This frequency is a solution to equation $\partial\,\mathrm{Im}(\tilde{Z}_{icl})/\partial\tilde{\omega} = 0$. The dependence of $\tilde{\omega}_{max}$ on k_σ is depicted in Fig. 5; this function is well approximated by

$$\tilde{\omega}_{max}(k_\sigma) = \frac{\tilde{\omega}_{max}^{\infty}}{1+1/k_\sigma}, \quad \tilde{\omega}_{max}^{\infty} = 10.162588 \qquad [39]$$

(solid line in Fig. 5). Here, $\tilde{\omega}_{max}^{\infty}$ is a solution to equation $\partial\,\mathrm{Im}(\tilde{Z}_{icl})/\partial\tilde{\omega} = 0$ at $k_\sigma \to \infty$. The high quality of fitting in Fig. 5 suggests that Eq. 39 is the exact result; however, this statement needs to be proved. The values of $\tilde{\omega}_{max}(k_\sigma)$ in the range of k_σ shown in Fig. 5 are the most interesting for applications.

In the dimension form, the relation between ω_{max} and k_σ is given by

$$\omega_{max} = \left(\frac{\sigma_p}{C_{dl} l_t^2}\right)\tilde{\omega}_{max}(k_\sigma) \qquad [40]$$

From Eqs. 31 and 39 it follows that finite electron conductivity of the ICL expands the diameter of Nyquist spectrum by the factor $(1+1/k_\sigma)$ and it lowers the summit frequency by the same factor.

Electronic impedance of inactive CL.—The leading terms in asymptotic expansion of the ICL impedance, Eq. 26, over large k_σ are

$$\tilde{Z}_{icl}^{k_\sigma\to\infty} \simeq \frac{1}{1+k_\sigma} + \frac{2(\cosh\varphi - 1)}{\varphi\sinh\varphi} + \frac{1}{k_\sigma(1+\cosh\varphi)} \times\left(1-\frac{3\sinh\varphi}{\varphi}\right), \quad \varphi = \sqrt{\mathrm{i}\tilde{\omega}} \qquad [41]$$

where the first term describing the HFR is taken from Eq. 26 unmodified.

The second term in Eq. 41 is the pure protonic impedance, Eq. 27. Thus, the last term in Eq. 41 is the approximate asymptotic expression for the electronic ICL impedance:

$$\tilde{Z}_{icl,e}^{k_\sigma\gg 1} \simeq \frac{1}{k_\sigma(1+\cosh\varphi)}\left(1-\frac{3\sinh\varphi}{\varphi}\right), \quad \varphi = \sqrt{\mathrm{i}\tilde{\omega}} \qquad [42]$$

Nyquist spectrum of electronic impedance $\tilde{Z}_{icl,e}^{k_\sigma\gg 1}$ multiplied by k_σ is shown in Fig. 6. Imaginary part of impedance is positive, which formally corresponds to negative capacitance of electrons, i.e.,

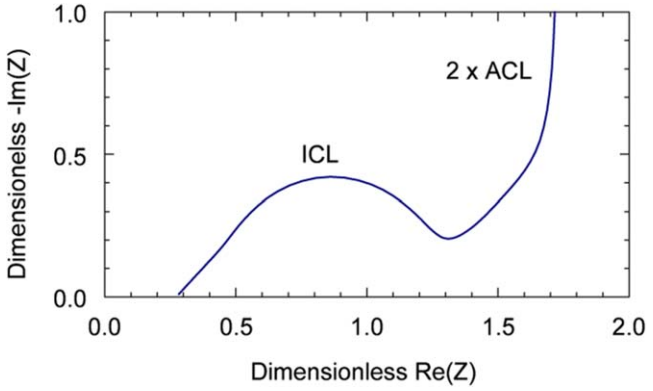

Figure 8. Nyquist spectrum of the ICL clamped between two ACLs. Ohmic contribution of the membranes is ignored. Thickness of the ICL is ten times less than the ACLs thickess.

protons increase the phase shift between AC potential and current, while electrons reduce this shift. More interesting is that the real component of $\tilde{Z}_{icl,e}^{k_\sigma \gg 1}$ is negative meaning that the electronic contribution to the polarization resistivity is negative.

From Eq. 31 it follows, that in systems with very low electronic conductivity, R_{icl}^{pol} tends to zero due to electronic component, while HFR increases. In other words, ICL with low σ_e transports protons without significant polarization resistivity. This is quite analogous to proton transport in a bulk membrane; indeed, the only resistive component of a system with poor σ_e is high–frequency resistivity $R_{icl}^{hfr} = l_t/\sigma_p$, as Eq. 32 shows. Evolution of the ICL spectrum, Eq. 26, as k_σ decreases is illustrated in Fig. 7. The spectrum for k_σ=0.1 is close to the "spectrum" of bulk membrane.

Experiment: inactive CL between two active CLs.—In experiments,[16] ICL was sandwiched between two membranes, and this package was inserted between two active catalyst layers to provide constant proton current through the ICL. The whole system was operated in hydrogen pumping regime, i.e., protons generated on one side of the cell moved through the ICL to another side, where they were converted back to hydrogen. Quite evidently, impedance of this system includes impedances of the HOR and HER electrodes. Impedance of each active layer is described by Eq. 21; for the whole system impedance we get

$$\tilde{Z}_{sys} = 2\tilde{Z}_{acl} + \tilde{Z}_{icl} + \tilde{R}_\Omega \qquad [43]$$

where $\tilde{R}_\Omega$ is the sum of the contact and membrane ohmic resistivities.

Generally, the ACLs' transport parameters may differ from the ICL parameters and using Eqs. 21, 26, we write

$$\tilde{Z}_{sys} = 2\left(\frac{1}{1+k_\sigma^*} + \frac{2+(k_\sigma^* + 1/k_\sigma^*)\cosh\xi^*}{(1+k_\sigma^*)\xi^*\sinh\xi^*}\right) + \left(\frac{1}{1+k_\sigma} + \frac{2k_\sigma(\cosh(\xi)-1)}{(1+k_\sigma)\xi\sinh\xi}\right) + \tilde{R}_\Omega \qquad [44]$$

where k_σ^* denotes the ratio σ_e^*/σ_p^* in the ACLs, and

$$\xi^* = \sqrt{\mathrm{i}\gamma\tilde{\omega}\left(1+\frac{1}{k_\sigma^*}\right)}, \quad \gamma = \frac{C_{dl}^*(l_t^*)^2/\sigma_p^*}{C_{dl}l_t^2/\sigma_p}. \qquad [45]$$

Here, the superscript * marks the ACL parameters. Equation 45 shows that the factor γ rescales frequency in the first term in Eq. 44. Assuming that the ACLs thickness is much larger than the ICL thickness, while the other parameters are of the same order of magnitude, from Eq. 45 it follows that $\gamma \gg 1$. Qualitatively it is clear, that the ACLs spectra would be shifted to the region of small frequencies compared to the ICL spectrum. Note that using ACLs of the same as ICL thickness would lead to overlapping of ACL and ICL spectra.

The Nyquist spectrum of the whole system $\tilde{Z}_{sys}$ for the case of $l_t/l_{t,*} = 10$ and $k_\sigma^* = k_\sigma = 10$ is shown in Fig. 8. The ICL arc is well pronounced in this case and the ICL polarization resistivity can be estimated with 10% accuracy by a naked eye ($\tilde{R}_{icl}^{pol} \simeq 1.3$?–? $0.3 = 1.0$, while the exact result is $1 - 1/11 \simeq 0.9$). Equation 45 shows that the higher γ, the better separation of ACL and ICL spectra on the frequency scale.

Conclusions

A physics–based model for impedance of inactive catalyst layer in Fig. 1b is developed. The model takes into account finite electron conductivity of the ICL. Analytical solution for ICL impedance is derived and expressions for the ICL high–frequency resistivity, polarization resistivity and for the summit frequency of the Nyquist

Table A·I. Main equations in the dimension form.

Equations	Dimension form
Equation 26	$Z_{icl} = \frac{l_t}{\sigma_p+\sigma_e} + \frac{2l_t(\cosh(\xi)-1)}{\sigma_p(1+\sigma_p/\sigma_e)\xi\sinh\xi}$, $\xi = \sqrt{\frac{\mathrm{i}\omega C_{dl}l_t^2}{\sigma_p}\left(1+\frac{\sigma_p}{\sigma_e}\right)}$
Equation 27	$Z_{icl}^{\sigma_e=\infty} = \frac{2l_t(\cosh(\sqrt{\mathrm{i}\tilde{\omega}})-1)}{\sigma_p\sqrt{\mathrm{i}\tilde{\omega}}\sinh\sqrt{\mathrm{i}\tilde{\omega}}}$, $\tilde{\omega} = \frac{\omega C_{dl}l_t^2}{\sigma_p}$
Equation 35	$Z_{icl,re}^{\omega\to\infty} \simeq \frac{l_t}{\sigma_p+\sigma_e} + \frac{l_t}{\sigma_p}\left(1+\frac{\sigma_p}{\sigma_e}\right)^{-3/2}\sqrt{\frac{2\sigma_p}{\omega C_{dl}l_t^2}}$
Equation 36	$Z_{icl,im}^{\omega\to\infty} \simeq \frac{l_t}{\sigma_p}\left(1+\frac{\sigma_p}{\sigma_e}\right)^{-3/2}\sqrt{\frac{2\sigma_p}{\omega C_{dl}l_t^2}}$
Equation 39	$\omega_{\max} = \left(\frac{\sigma_p}{C_{dl}l_t^2}\right)\frac{10.1626}{1+\sigma_p/\sigma_e}$
Equation 42	$Z_{icl,e}^{\sigma_e\gg\sigma_p} \simeq \frac{l_t}{\sigma_e(1+\cosh\varphi)}\left(1-\frac{3\sinh\varphi}{\varphi}\right)$, $\varphi = \sqrt{\frac{\mathrm{i}\omega C_{dl}l_t^2}{\sigma_p}}$

spectrum are obtained. Analytical solution for electron impedance of the system is obtained in the limit of large ratio of ICL electron and proton conductivities. Analytical expression for the ICL impedance can be used for fitting experimental impedance spectra. Analytical formulas for characteristic points of the ICL spectrum can be used for fast evaluation of ICL transport parameters without curve fitting (see Table A·I below).

Appendix A: Main Results in the Dimension Form

Table A·I displays the main results of this work in the dimension form suitable for processing experimental impedance spectra of the ICL.

ORCID

Andrei Kulikovsky https://orcid.org/0000-0003-1319-576X

References

1. M. Eikerling and A. A. Kornyshev, "Modelling the performance of the cathode catalyst layer of polymer electrolyte fuel cells." *J. Electroanal. Chem.*, **453**, 89 (1998).
2. A. A. Kulikovsky, "The regimes of catalyst layer operation in a fuel cell." *Electrochim. Acta*, **55**, 6391 (2010).
3. Zh. Tang, Q.-A. Huang, Y.-J. Wang, F. Zhang, W. Li, A. Li, L. Zhang, and J. J. Zhang, "Recent progress in the use of electrochemical impedance spectroscopy for the measurement, monitoring, diagnosis and optimization of proton exchange membrane fuel cell performance." *J. Power Sources*, **468**, 228361 (2020).
4. M. Ahadi, M. Tam, J. Stumper, and M. Bahrami, "Electronic conductivity of catalyst layers of polymer electrolyte membrane fuel cells: through-plane vs in-plane." *Int. J. Hydrogen Energy*, **44**, 3603 (2019).
5. T. Reshetenko, A. Serov, M. Odgaard, G. Randolf, L. Osmieri, and A. Kulikovsky, "Electron and proton conductivity of Fe-N-C cathodes for PEM fuel cells: a model–based electrochemical impedance spectroscopy measurement." *Electrochem. Comm.*, **118**, 106795 (2020).
6. M. Mandal, M. Moore, and M. Secanell, "Measurement of the protonic and electronic conductivities of PEM water electrolyzer electrodes." *ACS Appl. Mater. Interfaces*, **12**, 49549 (2020).
7. T. Schuler, J. M. Ciccone, B. Krentscher, F. Marone, C. Peter, T. J. Schmidt, and F. N. Büchi, "Hierarchically structured porous transport layers for polymer electrolyte water electrolysis." *Adv. Energy Mater.*, **10**, 1903216 (2020).
8. G. Yang, S. Yu, Z. Kang, Y. Li, G. Bender, B. S. Pivovar, J. B. Green Jr., D. A. Cullen, and F.-Y. Zhang, "Building electron/proton nanohighways for full utilization of water splitting catalysts." *Adv. Energy Mater.*, **10**, 1903871 (2020).
9. A. Kosakian and M. Secanell, "Estimating charge-transport properties of fuel-cell and electrolyzer catalyst layers via electrochemical impedance spectroscopy." *Electrochim. Acta*, **367**, 137521 (2021).
10. J. H. Jang, S. Jeon, J. H. Cho, S.-K. Kim, E. Cho, S.-Y. Lee, H.-J. Kim, J. Han, and T.-H. Lim, "Complex capacitance analysis of ionic resistance in PEMFC and DMFC catalyst layers." *J. Electrochem. Soc.*, **156**, B1293 (2009).
11. Y. Liu, W. Gu, D. R. Baker, J. Jorne, and H. A. Gasteiger, "Proton conduction in pem fuel cell cathodes: effects of electrode thickness and ionomer equivalent weight." *J. Electrochem. Soc.*, **157**, B1154 (2010).
12. Y. Liu, C. Li, W. Gu, J. Jorne, and H. A. Gasteiger, "Effects of catalyst carbon support on proton conduction and cathode performance in pem fuel cells." *J. Electrochem. Soc.*, **158**, B614 (2011).
13. R. Makharia, M. F. Mathias, and D. R. Baker, "Measurement of catalyst layer electrolyte resistance in PEFCs using electrochemical impedance spectroscopy." *J. Electrochem. Soc.*, **152**, A970 (2005).
14. D. Malevich, B. R. Jayasankar, E. Halliop, J. G. Pharoah, B. A. Peppley, and K. Karan, "On the determination of PEM fuel cell catalyst layer resistance from impedance measurement in H2/N2 cells." *J. Electrochem. Soc.*, **159**, F888 (2012).
15. M. Obermaier, A. S. Bandarenka, and C. Lohri-Tymozhynsky, "A comprehensive physical impedance model of polymer electrolyte fuel cell cathodes in oxygen-free atmosphere." *Sci. Reports*, **8**, 4933 (2018).
16. D. C. Sabarirajan, J. Liu, Y. Qi, A. Perego, A. T. Haug, and I. V. Zenyuk, "Determining proton transport in pseudo catalyst layers using hydrogen pump DC and AC techniques." *J. Electrochem. Soc.*, **167**, 084521 (2020).
17. J. Huang, Y. Gao, J. Luo, S. Wang, C. Li, S. Chen, and J. Zhang, "Editors' choice-review-impedance response of porous electrodes: theoretical framework, physical models and applications." *J. Electrochem. Soc.*, **167**, 166503 (2020).
18. C. Boyer, S. Gamburzev, O. Velev, S. Srinivasan, and A. J. Appleby, "Measurements of proton conductivity in the active layer of PEM fuel cell gas diffusion electrodes." *Electrochimica Acta*, **24**, 3703 (1998).
19. H. Iden, A. Ohma, and K. Shinohara, "Analysis of proton transport in pseudo catalyst layers." *J. Electrochem. Soc.*, **156**, B1078 (2009).
20. H. Iden, K. Sato, A. Ohma, and K. Shinohara, "Relationship among microstructure, ionomer property and proton transport in pseudo catalyst layers." *J. Electrochem. Soc.*, **158**, B987 (2011).
21. D. Kramer, S. A. Freunberger, R. Flückiger, I. A. Schneider, A. Wokaun, F. N. Büchi, and G. G. Scherer, "Electrochemical diffusimetry of fuel cell gas diffusion layers." *J. Electroanal. Chem.*, **612**, 63 (2008).
22. D. Macdonald, "Reflections on the history of electrochemical impedance spectroscopy." *Electrochim. Acta*, **51**, 1376 (2006).
23. A. Kulikovsky, "Analysis of proton and electron transport impedance of a PEM fuel cell in H_2/N_2 regime." *Electrochem. Sci. Adv.*, e202000023 (2020).